

SpliceRadar: A Learned Method For Blind Image Forensics

Aurobrata Ghosh¹ Zheng Zhong¹ Terrance E Boulton² Maneesh Singh¹
¹Verisk AI, Verisk Analytics ²Vision and Security Technology (VAST) Lab

{aurobrata.ghosh, zheng.zhong, maneesh.singh}@verisk.com tboulton@vast.uccs.edu

Abstract

Detection and localization of image manipulations like splices are gaining in importance with the easy accessibility to image editing softwares. While detection generates a verdict for an image it provides no insight into the manipulation. Localization helps explain a positive detection by identifying the pixels of the image which have been tampered. We propose a deep learning based method for splice localization without prior knowledge of a test image's camera-model. It comprises a novel approach for learning rich filters and for suppressing image-edges. Additionally, we train our model on a surrogate task of camera model identification, which allows us to leverage large and widely available, unmanipulated, camera-tagged image databases. During inference, we assume that the spliced and host regions come from different camera-models and we segment these regions using a Gaussian-mixture model. Experiments on three test databases demonstrate results on par with and above the state-of-the-art and a good generalization ability to unknown datasets.

1. Introduction

“A picture is worth a thousand words”. A statement, which appeared in print in the early 1900s, has become a ubiquitous part of our daily lives with the advance of camera technology. Ironically, however, with media becoming digitized, this implicit trust is under attack. With the accessibility of image editing softwares and wide diffusion of digital images over the internet, anyone can easily create and distribute convincing fake pictures. These fakes have a significant impact on our lives: from the private, the social, to the legal. It is imperative, therefore, to develop digital forensic tools capable of detecting such fakes.

Typically, a fake well done hides its manipulations cleverly with the semantic contents of the image, therefore, forensic algorithms inspect low-level statistics of images or inconsistencies therein to identify manipulations. These include distinctive features stemming from the hardware and software of a particular camera make (or a post-processing

step thereafter). For example, at the lowest hardware level, the photo-response non-uniformity (PRNU) noise pattern is a digital noise “fingerprint” of a particular device and can be used for camera identification [8]. The colour filter array (CFA) and its interpolation algorithms are also particular to a device and can help discern between cameras [22]. At a higher level, the image compression format, *e.g.* the popular JPEG format, can help determine single versus multiple compressions [3] or different device makes [26, 23]. This is useful in the detection of digital edits and localization of splices [1].

Traditional image forensic algorithms have modelled discrepancies in one or multiple such statistics to detect or localize splicing manipulations. Prior knowledge characterizing these discrepancies have been leveraged to design handcrafted features. The survey in [27] compares the performances of a number of such algorithms.

Learned forensic approaches have recently gained popularity with the growing success of machine learning and deep learning. In [10], Cozzolino *et al.* recast hand designed high pass filters, useful for extracting residual signatures, as a constrained CNN to learn the filters and residuals from a training dataset. Zhou *et al.* [28], proposed a dual branch CNN, one learning from the image-semantic and the other learning from the image-noise, to localize spliced regions. Huh *et al.* [18] (henceforth referred to as EXIF-SC), leveraged the EXIF metadata to train a Siamese neural network to verify metadata consistency among patches of a test image to localize manipulated pixels. In [24], Rössler *et al.* took on a new genre of forensic attacks – state-of-the-art face manipulations including some created by deep neural networks – and showed that learned CNNs outperformed traditional methods. However, their success notwithstanding, deep learning approaches have typically shown vulnerability to generalizing to new datasets [11, 2, 25].

In this paper, we propose a novel, blind forensic approach based on CNNs to localize spliced regions in an image without any prior knowledge of the source cameras. We employ a new way to learn high pass “rich” filters and a novel probabilistic regularization based on mutual information to suppress semantic contents in the training images

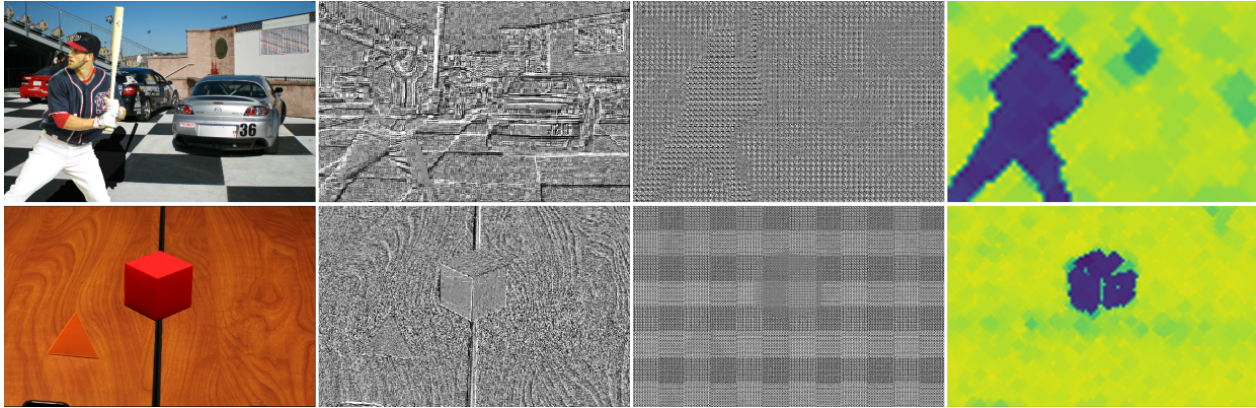


Figure 1. *SpliceRadar* is able to learn low level features while suppressing semantic-information which are image specific. This allows it to generalize well to new tampered datasets. Two examples: col-1: input image, col-2: sample of a learned rich filter (contains semantic-edges), col-3: final features (semantic-edges suppressed), col-4: output heat map indicating tampered region.

and learn low-level features of camera models. Our network is trained for a surrogate task of source-camera identification, which allows us to use large, widely available camera-tagged untampered images for training. Forgery localization is done by computing the low-level features of the image, which identifies the signatures of multiple source camera models, and segmenting these regions using a Gaussian mixture model. Preliminary results from a number of test databases: DSO-1 [13], Nimble Challenge 2016 (NC16) and Nimble Challenge 2017 (NC17-dev1) [14] show an improvement over the state-of-the-art. Furthermore, since our training data is unrelated to the test datasets, it also demonstrates good generalization ability.

In summary, the contributions in this paper are:

- a new way to learn high pass rich filters using constrained CNNs that compute residuals, highlighting low-level information over the semantics of the image;
- a novel probabilistic regularization based on mutual information, which helps to suppress image-edges in the training data;
- experimental analysis showing up to $\sim 4\%$ (points) improvement over the state-of-the-art on three standard test datasets: DSO-1, NC16 and NC17-dev1.

2. Related Work

Rich Filters: Spatial rich models for steganalysis [15], proposed a large set of hand-engineered high pass filters, *rich filters* (RFs), to extract local noise-like features from an image. By computing dependencies among neighbouring pixels, these filters draw out residual information that highlights low-level statistics over the image-semantics. Rich filters have proven extremely effective in image forensics and have been widely adopted by various state-of-the-art

splice detection algorithms. SpliceBuster (SB) [9], a blind splice detection algorithm, used one such fixed filter to separate camera features from the spliced and host regions. In [28], three fixed rich filters were used in the noise-branch to compute residuals along with a CNN to learn co-occurrence probabilities of the residuals as features to train a region proposal network to detect spliced regions. Bayar and Stamm [4, 5], proposed a constrained convolution layer to learn RF-like features and a CNN to learn the co-occurrence probabilities from the data. At every iteration they projected the weights of the constrained layer to satisfy $\mathbf{w}_k(0, 0) = -1$ and $\sum_{m,n \neq 0,0} \mathbf{w}_k(m, n) = 1$, where $\mathbf{w}_k(i, j)$ is the weight of the k^{th} filter at position (i, j) . The end-to-end trained network in [5] was used to identify broad image-level manipulations like blurring and compression. We also use learned RFs but propose a new constrained convolution layer and a different approach to applying the constraints.

Camera Identification: Camera identification plays an important part in image forensics. Lukas *et al.* proposed a PRNU based camera identification algorithm in [19] where they estimated nine reference noise patterns using wavelet denoising and averaging, then matched the reference patterns to new images by correlation to determine the source camera. CNNs were trained to compute features along with SVMs for source camera identification in [6]. Learned RFs from constrained convolution layers were used for camera identification in [4]. Recently, Mayer and Stamm [21], trained a similar learned RF based CNN for a camera identification task, then used the output of the CNN as features to train a second network for splice detection. In [7], Bondi *et al.* proposed a strategy similar to ours in spirit: a CNN as a feature extractor to identify camera-models, patch based feature computation of a test image and clustering of the patch-features to localize spliced regions. However, it is

fundamentally different from our proposed method. Bondi *et al.* used regular convolutions and max-pooling in their CNN, which are typically used to learn high-level semantic structures of an image, therefore biasing the CNN to learn semantic contents of the training data. In this work, we propose to suppress the semantic contents of an image to learn the distinguishing low-level features of a camera-model. Additionally, the experiments in [7] are conducted on synthetic datasets with straightforward manipulations. In comparison, we demonstrate our method on multiple established test datasets with (series of) complex manipulations.

3. Proposed Method

We propose *SpliceRadar* (SR), a deep learning approach for blind forgery localization. Our network has no prior knowledge of the source cameras of either the host or the spliced image regions. Instead, it is trained to compute low-level features which can segregate camera-models. A tampered region is localized by computing the features over the entire image and then segmenting the feature-image using a Gaussian mixture model.

We train our network to differentiate camera-models instead of individual device instances. The learned features contain signatures of the entire image formation pipeline of a camera-model: from the hardware, the internal processing algorithms, to the compression.

Although challenging, we choose a blind localization strategy to improve the generalization ability of our network. This is achieved by training the SpliceRadar network on a surrogate task of source camera-model identification, which allows us to leverage large and widely available camera-tagged image databases. It also allows us to avoid known manipulated datasets and risk the chance of over-specializing towards these. Additionally, we train with a large number of camera models. This helps not only to generalize better but also to boost our network’s ability to segregate camera models. This ability to differentiate (even unknown) camera-models is of greater interest to us than the ability to identify the models available during training.

Low-level features: A key contribution in our design of SpliceRadar is its ability to learn low-level features independent of the image-semantics. This is achieved in our architecture by a two-step process: residual information extraction and semantic-edge suppression. The first layer of the network consists of a set of learned RFs comparable to [4, 5]. These largely suppress the semantic contents of an input patch from a colour-image by learning to compute residuals. However, since RFs are high-pass filters they also accentuate the semantic-edges present in the image (see Fig. 1). Searching for patterns based on these will likely lead to learning misleading image specific information that is not truly independent of the semantics. This will result in our network learning information specific to

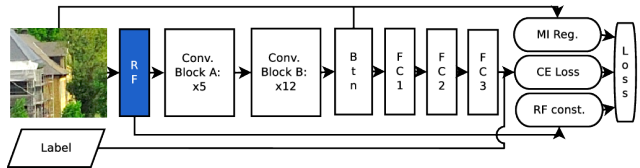


Figure 2. System architecture of SpliceRadar.

the semantic contents of the training data, which would affect its generalization ability. Therefore, after learning the spatial distribution of these residuals, we further suppress the remaining semantic-edges by applying a probabilistic regularization. From these we learn a hundred-dimensional feature vector characteristic of a camera-model and independent of the image-semantics. These features are used to drive a cross-entropy loss during training and for segmentation during forgery localization.

Learned RFs: The first layer of our network computes residuals from learned filters that resemble RFs in [15]. We propose a novel way to do this using constrained convolutions that is different from [4, 5]. Developing along the lines of the original hand engineered RFs [15], we define a residual to be the difference between a predicted value for a central pixel defined over its neighbourhood and the scaled value of the pixel. Therefore, from Eq. 1 in [15], we propose the constrained convolution to learn residuals as:

$$\mathcal{R}_{RF}^{(k)} = \mathbf{w}_k(0, 0) + \sum_{m, n \neq 0, 0} \mathbf{w}_k(m, n) = 0, \quad (1)$$

for the k^{th} filter, where the support of the residuals is a $N \times N$ neighbourhood ($N = 5$). The summation ensures that the predicted value and the pixel’s value have opposite signs [15]. Following the spirit of the original work, we propose to use a large bank of learned RFs, $k = 1..64$, instead of only 3 learned RFs like in [4, 5]. These constraints are applied by including $\mathcal{R}_{RF} = (\sum_k (\mathcal{R}_{RF}^{(k)})^2)^{\frac{1}{2}}$ as a penalty in the cost function. This allows our network to learn suitable residuals for camera-model classification.

System architecture: We propose an eighteen layer deep CNN that takes as input a $72 \times 72 \times 3$ RGB patch, and the camera-model label during training, as shown in Fig. 2. The first layer is a constrained convolution layer with kernel size $5 \times 5 \times 3 \times 64$, producing 64 filters as described above. Convolution block A comprises of a convolution without padding with kernel size $3 \times 3 \times X \times 19$, batch-normalization and ReLU activation. It is repeated five times, with $X = 64$ the first time and then 19. Convolution block B comprises of two identical sub-blocks and a skip-connection around the second sub-block. Each sub-block consists of a convolution with padding with kernel size $3 \times 3 \times 19 \times 19$, batch-normalization and ReLU activation. The skip-connection adds the output of the first sub-block’s ReLU activation to

the output of the second sub-block’s batch-normalization. This is repeated twelve times. We found this architecture to be more effective than a standard residual block [17], since it achieved $\sim 10\%$ better validation accuracy at the surrogate task of camera-model identification during training. The two convolution blocks together learn the spatial distribution of residual values and can be interpreted as learning their co-occurrences. The final “bottleneck” convolution has kernel size $3 \times 3 \times 19 \times 1$. Its output is a *pre-feature image* of size 56×56 . All convolutions have stride 1. Following these are three fully-connected layers: FC1 with 75 neurons, FC2, the *feature-layer*, with 100 neurons, and FC3, the final layer that outputs logits, with a number of neurons, C , corresponding to the number of training camera models. FC1 is followed by a dropout layer with keep-probability of 0.8 and ReLU non-linearity. The network is trained using cross-entropy loss over the training data:

$$\mathcal{L}_{CE} = -\frac{1}{M} \sum_{i=1}^M \mathbf{y}_i \log(\hat{\mathbf{y}}_i), \quad (2)$$

where \mathbf{y}_i is the camera-model label for the i^{th} training data point in the mini-batch of length M and $\hat{\mathbf{y}}_i$ is the softmax value computed from the output of FC3.

Mutual Information based regularization: Mutual information (MI) is a popular metric for registering medical images since it captures linear and non-linear dependencies between two random variables and can effectively compare images of the same body part across different modalities with different contrasts (*e.g.* MRI, CT, PET) [20]. We take advantage of this property of MI to compute the dependency of the input patch, \mathbf{P}_i , with the pre-feature image, \mathbf{p}_i , which is the output of the final convolution layer, although they may have different dynamic contrast ranges. Given that \mathbf{p}_i is a transformed version of the residuals computed by the first layer, the dependency primarily reflects the presence of semantic-edges in \mathbf{p}_i . Therefore, we consider:

$$\mathcal{R}_{MI} = \frac{1}{M} \sum_{i=1}^M \text{MI}(\rho(\mathbf{P}_i), \mathbf{p}_i), \quad (3)$$

as a regularization, where $\rho(\cdot)$ allows to approximate MI numerically and is described below.

The complete loss function for training our network combines these various components and also includes l_2 regularization of all weights, \mathbf{W} , of the network:

$$\mathcal{L} = \mathcal{L}_{CE} + \lambda \mathcal{R}_{RF} + \gamma \mathcal{R}_{MI} + \omega \|\mathbf{W}\|_2, \quad (4)$$

where λ , γ and ω balance the amount of RF constraint penalty and MI & l_2 regularizations to apply along with the main loss.

Splice localization: We assume that that genuine part of the image comes from a single camera-model and has the

Dataset	#Img.	Format
DSO-1 [13]	100	PNG
NC16 [14]	564	JPEG (mostly)
NC17-dev1 [14]	1191	JPEG (mostly)

Table 1. Details of test datasets we consider.

largest number of pixels, while the spliced region(s) is smaller in comparison. Therefore, we simplify the localization task to a two-class segmentation problem, where the distributions of both the classes are approximated by Gaussian distributions and the smaller class represents the departure from the feature-statistics of the larger genuine class.

First, we subdivide the test image into $72 \times 72 \times 3$ sized patches and compute the feature vector, FC2, for each patch. The amount of overlap between neighbouring patches is a hyper-parameter we discuss later. Then, we run an expectation-maximization (EM) algorithm to fit a two-component Gaussian mixture model to the feature-vectors, to segregate the patches into two classes. We rerun this fitting one hundred times with random initializations and select the solution with the highest likelihood. This probability map is first “cleaned” of spurious noise using morphological opening (or closing) operation using a fixed disk of size two. Then it is upsampled to the original image’s dimensions and used for localizing the tampered region(s).

3.1. Implementation Details

Training: We trained our network using the Dresden Image Database (B) [16], which comprises of $C = 27$ camera-models and almost 17,000 JPEG images. We did not segregate the images by their compression quality-factors as we considered these to be part of the camera models signature. For each camera-model we randomly selected 0.2% and 0.1% of the images as validation and test sets, while the remaining files were used for training. The training comprised of a mini-batch size of $M = 50$ patches and 100,000 patches per epoch chosen randomly every epoch. The network was trained for 130 epochs, using Adam optimizer with a constant learning rate of $1e - 4$ for 80 epochs and then decaying exponentially by a factor of 0.9 over the remaining epochs. This took approximately two days on an NVIDIA GTX 1080Ti GPU for our TensorFlow based implementation. We obtained optimal results of $\sim 72\%$ camera-model identification accuracy on the validation and test sets for weights (Eq. 4): $\lambda = \gamma = 1$ and $\omega = 5e - 4$, which were found empirically.

MI: We computed the MI in Eq. 3 numerically by approximating $p(\rho(\mathbf{P}_i))$, $p(\mathbf{p}_i)$ and $p(\rho(\mathbf{P}_i), \mathbf{p}_i)$ the marginal and joint distributions of \mathbf{P}_i and \mathbf{p}_i , using histograms (50 bins). To do this, we defined $\rho(\cdot)$ as a transform that first converts \mathbf{P}_i ($72 \times 72 \times 3$) to its gray-scalar version then resizes it to the dimensions of \mathbf{p}_i (56×56). $\rho(\cdot)$ conserves the semantic-edges in \mathbf{P}_i and aligns them to the edges in \mathbf{p}_i . Histogram

Step (pixels)	F1	MCC	ROC AUC
24	0.59	0.53	0.85
36	0.65	0.61	0.89
48	0.69	0.65	0.91
60	0.68	0.64	0.91
72	0.67	0.64	0.90

Table 2. Overlap hyper-parameter search on DSO-1. Best results are achieved for a step of 48 pixels.

based MI computation is a common approximation that is widely used in medical imaging [20]. However, it is also computationally inefficient, which explains the long training time.

4. Results

We now demonstrate our proposed method for blind splice detection. To evaluate its performance quantitatively, we conduct experiments on three datasets, use three pixel-level scoring metrics, and compare against two top performing splice detection algorithms. Additionally, we also present the results of a hyper-parameter search to decide on the optimal overlap of patches during inference (splice localization).

The datasets we select are DSO-1, NC16 and NC17-dev1 (Table 1). These recent datasets contain realistic manipulations that are challenging to detect. DSO-1 contains splicing manipulations, where human figures, in whole or in parts, have been inserted into images of other people. NC16 and NC17-dev1 are more complex and challenging datasets. Images from these may contain a series of manipulations that may span the entire image or a relatively small region. Furthermore, some of these manipulations may be post-processing operations that are meant to make forgery detection more difficult. All three datasets provide binary ground-truth manipulation masks.

To evaluate the performance quantitatively we consider: F1 score, Matthews Correlation Coefficient (MCC) and area under the receiver operating characteristic curve (ROC-AUC). These metrics have been adopted widely by the digital image forensics community [27, 12]. Since our proposed method generates a probability map, F1 and MCC require a threshold to compute a pixel-level binary mask. Again, as per common practice, we report the values of these scores for the optimal threshold, which is computed with reference to the ground-truth manipulation mask [28, 25, 12].

We compare our approach with two state-of-the-art algorithms: SB and EXIF-SC. SB [9], as discussed above, uses the co-occurrences of a residual computed from a single hand-engineered RF and EM algorithm for splice localization. It is also a blind approach which has proven its merit as a top performer in the 2017 Nimble Challenge. EXIF-SC

Step (pixels)	F1	MCC	ROC AUC
24	0.18	0.12	0.64
36	0.19	0.13	0.65
48	0.45	0.41	0.81
60	0.4	0.36	0.78
72	0.22	0.17	0.67

Table 3. Overlap hyper-parameter search on 100 randomly selected test images from NC16. Best results are achieved for a step of 48 pixels.

Step (pixels)	F1	MCC	ROC AUC
24	0.33	0.17	0.70
36	0.34	0.19	0.71
48	0.38	0.22	0.73
60	0.36	0.22	0.73
72	0.36	0.23	0.74

Table 4. Overlap hyper-parameter search on 100 randomly selected test images from NC17-dev1. Results achieved for a step of 48 pixels are comparable to the best results.

[18], is a recent publication that has demonstrated promising potential by applying a deep neural network to detect splices by predicting meta-data inconsistency. For each of these methods we report the scores that we computed in our experiments, using the original codes/models of the authors,¹ along with the scores reported by the authors.

First, we present the results of the hyper-parameter search to decide the optimal overlap of patches during inference. The overlap is computed in terms of pixels we step along an axis to move from one patch to the next. We compute the performance of our model for steps ranging from 24 to 72 pixels on the hundred images of DSO-1 and hundred random images of NC16 and NC17-dev1 each. The results are presented in Tables 2,3,4. From these we see that a step of 48 pixels produces favourable results consistently. Therefore, we consider 48 pixels as the optimal step size in all our experiments.

Next, we present the results of forgery detection. Table 5 presents the F1 scores achieved by all three algorithms over the three test datasets. SpliceRadar is able to improve over the performances of SB and EXIF-SC on DSO-1 and NC16, while its performance is on par with them on NC17-dev1. Table 6 presents the MCC results in a similar format. Again, SpliceRadar outperforms SB and EXIF-SC on DSO-1 and NC16 and ties with SB as a top performer on NC17-dev1. The ROC-AUC results are presented in Table 7. In this case, SpliceRadar has the best scores on all three datasets, indicating a better global performance across all thresholds.

¹<http://www.grip.unina.it/research/83-image-forensics/100-splicebuster.html>,
<https://minyoungg.github.io/selfconsistency/>

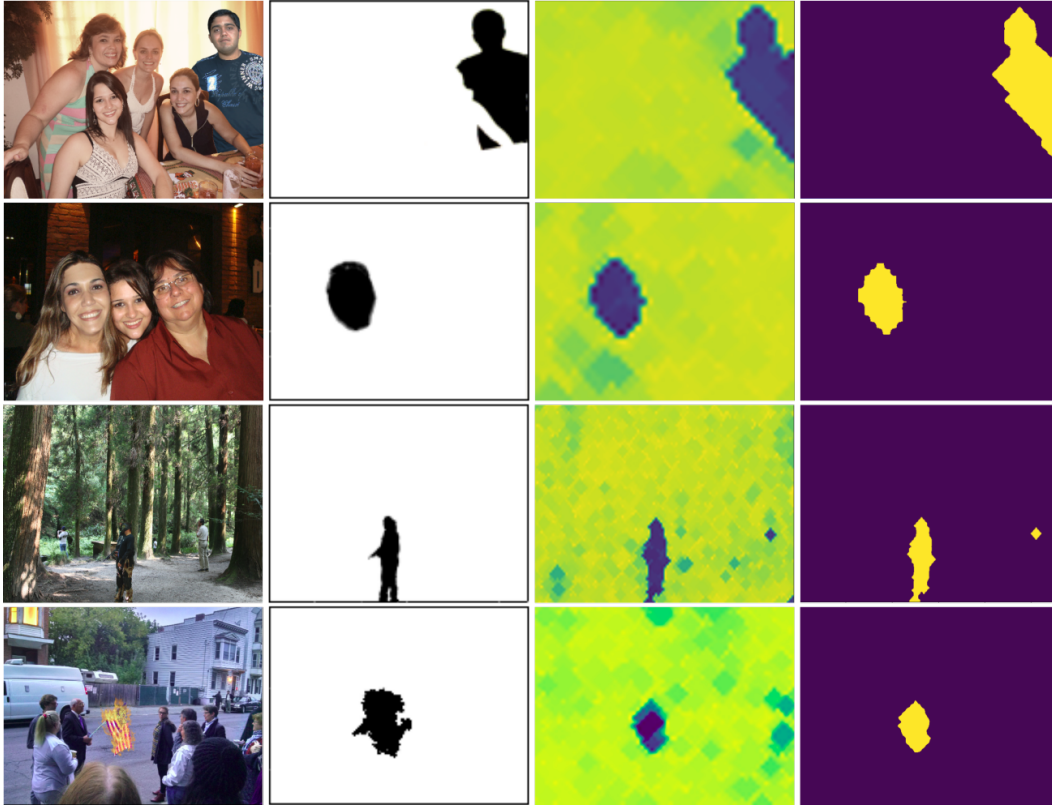


Figure 3. Qualitative results from SpliceRadar. Col-1: input image, col-2: ground-truth manipulation mask, col-3: predicted probability heat map, col-4: predicted binary mask. Rows-1,2: DSO-1, row-3: NC16, row-4: NC17-dev1.

	DSO-1	NC16	NC17-dev1
EXIF-SC	0.57 (0.52)	0.38	0.41
SB	0.66 (0.66)	0.37 (0.36)	0.43
SR	0.69	0.40	0.42

Table 5. Results: F1 score comparison on the test datasets. Black: scores we computed, blue: scores reported by the authors. (For SB, we cite results from [12]).

Overall, from these three tables, we observe that our proposed method’s performance is not only comparable to the state-of-the-art, but up to 4% points better.

We present qualitative results in Figs. 3,4, where we select examples from all three datasets DSO-1, NC16 and NC17-dev1. Fig. 3 shows the input colour image in the first column, the ground-truth manipulation mask in the second column, the probability heat map predicted by SpliceRadar in the third column and the predicted binarized manipulation mask in the final column. In Fig. 4, we qualitatively compare the predicted binarized masks of all three algorithms compared in Tables 5,6,7 alongside the input image and the ground-truth manipulation mask. These figures provide a visual insight into our method’s performance.

Finally, in Fig. 5 we present some hard examples, where

	DSO-1	NC16	NC17-dev1
EXIF-SC	0.52 (0.42)	0.36	0.18
SB	0.61 (0.61)	0.34 (0.34)	0.2
SR	0.65	0.38	0.2

Table 6. Results: MCC score comparison on the test datasets. Black: scores we computed, blue: scores reported by the authors. (For SB, we cite results from [12]).

	DSO-1	NC16	NC17-dev1
EXIF-SC	0.85	0.80	0.71
SB	0.86	0.77	0.69
SR	0.91	0.81	0.73

Table 7. Results: ROC-AUC score comparison on the test datasets.

all three algorithms fail to detect the spliced regions. These examples require further investigation and indicate future research directions.

5. Conclusion and Future Directions

We proposed a novel method for blind forgery localization using a deep convolutional neural network that learns low-level features capable of segregating camera-models.



Figure 4. Qualitative comparison of SpliceRadar, SB and EXIF-SC. Col-1: input image, col-2: ground-truth manipulation mask, col-3: mask from SB, col-4: mask from EXIF-SC, col-5: mask from SpliceRadar. Rows-1,2: NC16, rows-3,4: NC17-dev1.

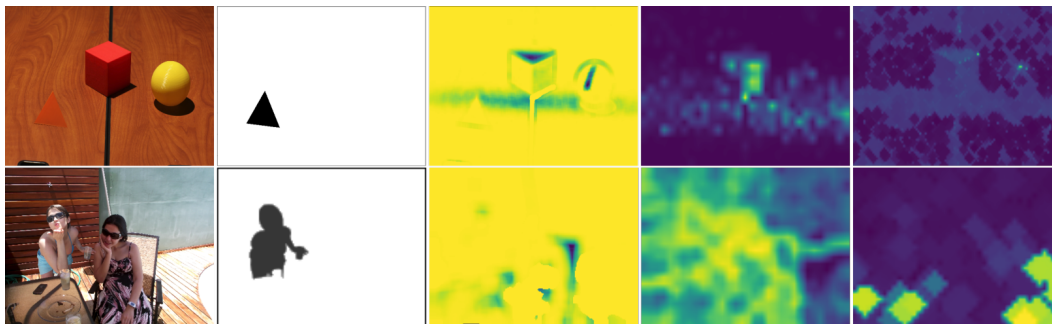


Figure 5. Hard examples where all three algorithms, SpliceRadar, SB and EXIF-SC, fail to detect the spliced regions. Col-1: input image, col-2: ground-truth manipulation mask, col-3: heat map from SB, col-4: heat map from EXIF-SC, col-5: heat map from SpliceRadar.

These low-level features, independent of the semantic contents of the training images, were learned in two stages: first, using our new constrained convolution approach to learn relevant residuals and second, using our novel probabilistic MI-based regularization to suppress semantic-edges. Preliminary results on three test datasets demonstrated the potential of our approach, indicating up to 4% points improvement over the state-of-the-art.

In this first study, we compared our approach with two top performing state-of-the-art methods on three datasets. We plan more extensive tests in the future with more recent datasets like those from Media Forensics Challenge 2018 and more algorithms. We plan to also systematically inves-

tigate the effects of JPEG compression.

One shortcoming of our approach is the histogram based implementation of mutual information, which is computationally cumbersome. This compelled us to curtail our model in a number of ways: to use a relatively small mini-batch size, to train for a limited number of epochs and to consider a relatively small network. We plan to improve this bottleneck in the future to enable us to train larger models on bigger datasets more efficiently. We also identified hard examples where all the algorithms we tested failed to identify the correct spliced regions. These require further investigation. Finally, we foresee including more prior knowledge to improve results, for example fine-tuning our model

on the training data provided with each dataset.

References

- [1] S. Agarwal and H. Farid. Photo forensics from JPEG dimples. In *2017 IEEE Workshop on Information Forensics and Security (WIFS)*, pages 1–6, 12 2017.
- [2] J. H. Bappy, A. K. Roy-Chowdhury, J. Bunk, L. Nataraj, and B. S. Manjunath. Exploiting spatial structure for localizing manipulated image regions. In *The IEEE International Conference on Computer Vision (ICCV)*, 10 2017.
- [3] M. Barni, E. Nowroozi, and B. Tondi. Higher-order, adversary-aware, double JPEG-detection via selected training on attacked samples. In *25th European Signal Processing Conference (EUSIPCO)*, pages 281 – 285, 08 2017.
- [4] B. Bayar and M. C. Stamm. Augmented convolutional feature maps for robust CNN-based camera model identification. In *2017 IEEE International Conference on Image Processing (ICIP)*, pages 4098–4102, 09 2017.
- [5] B. Bayar and M. C. Stamm. Constrained convolutional neural networks: A new approach towards general purpose image manipulation detection. *IEEE Transactions on Information Forensics and Security*, 13(11):2691–2706, 11 2018.
- [6] L. Bondi, L. Baroffio, D. Güera, P. Bestagini, E. J. Delp, and S. Tubaro. First steps toward camera model identification with convolutional neural networks. *IEEE Signal Processing Letters*, 24(3):259–263, 03 2017.
- [7] L. Bondi, S. Lamari, D. Güera, P. Bestagini, E. Delp, and S. Tubaro. Tampering detection and localization through clustering of camera-based CNN features. In *The IEEE Conference on Computer Vision and Pattern Recognition (CVPR)*, pages 1855–1864, 07 2017.
- [8] M. Chen, J. Fridrich, M. Goljan, and J. Luks. Determining image origin and integrity using sensor noise. *Information Forensics and Security, IEEE Transactions on*, 3:74 – 90, 04 2008.
- [9] D. Cozzolino, G. Poggi, and L. Verdoliva. Splicebuster: A new blind image splicing detector. In *2015 IEEE International Workshop on Information Forensics and Security (WIFS)*, pages 1–6, 11 2015.
- [10] D. Cozzolino, G. Poggi, and L. Verdoliva. Recasting residual-based local descriptors as convolutional neural networks: An application to image forgery detection. In *Proceedings of the 5th ACM Workshop on Information Hiding and Multimedia Security*, pages 159–164, New York, NY, USA, 2017. ACM.
- [11] D. Cozzolino, J. Thies, A. Rössler, C. Riess, M. Nießner, and L. Verdoliva. Forensictransfer: Weakly-supervised domain adaptation for forgery detection. *arXiv*, 2018.
- [12] D. Cozzolino and L. Verdoliva. Noiseprint: a CNN-based camera model fingerprint. *arXiv*, 2018.
- [13] T. J. d. Carvalho, C. Riess, E. Angelopoulou, H. Pedrini, and A. d. R. Rocha. Exposing digital image forgeries by illumination color classification. *IEEE Transactions on Information Forensics and Security*, 8(7):1182–1194, 07 2013.
- [14] J. Fiscus, H. Guan, Y. Lee, A. Yates, A. Delgado, D. Zhou, D. Joy, and A. Pereira. The 2017 Nimble Challenge Evaluation: Results and Future Directions, 2017.
- [15] J. Fridrich and J. Kodovsky. Rich models for steganalysis of digital images. *IEEE Transactions on Information Forensics and Security*, 7(3):868–882, 06 2012.
- [16] T. Gloe and R. Bhme. The ‘Dresden Image Database’ for benchmarking digital image forensics. In *Proceedings of the 25th Symposium On Applied Computing (ACM SAC 2010)*, volume 2, pages 1585–1591, 2010.
- [17] K. He, X. Zhang, S. Ren, and J. Sun. Deep residual learning for image recognition. In *The IEEE Conference on Computer Vision and Pattern Recognition (CVPR)*, pages 770–778, 06 2016.
- [18] M. Huh, A. Liu, A. Owens, and A. A. Efros. Fighting fake news: Image splice detection via learned self-consistency. In V. Ferrari, M. Hebert, C. Sminchisescu, and Y. Weiss, editors, *Computer Vision – ECCV*, pages 106–124, Cham, 2018. Springer International Publishing.
- [19] J. Lukas, J. Fridrich, and M. Goljan. Digital camera identification from sensor pattern noise. *IEEE Transactions on Information Forensics and Security*, 1(2):205–214, 06 2006.
- [20] F. Maes, D. Vandermeulen, and P. Suetens. Medical image registration using mutual information. *Proceedings of the IEEE*, 91(10):1699–1722, 10 2003.
- [21] O. Mayer and M. C. Stamm. Learned forensic source similarity for unknown camera models. In *IEEE International Conference on Acoustics, Speech and Signal Processing (ICASSP)*. IEEE SigPort, 2018.
- [22] A. C. Popescu and H. Farid. Exposing digital forgeries in color filter array interpolated images. *IEEE Transactions on Signal Processing*, 53(10):3948–3959, 10 2005.
- [23] T. Qiao, F. Reirant, R. Cogranne, and T. H. Thai. Individual camera device identification from JPEG images. *Signal Processing: Image Communication*, 52:74 – 86, 2017.
- [24] A. Rössler, D. Cozzolino, L. Verdoliva, C. Riess, J. Thies, and M. Nießner. Faceforensics++: Learning to detect manipulated facial images. *arXiv*, 2019.
- [25] R. Salloum, Y. Ren, and C.-C. J. Kuo. Image splicing localization using a multi-task fully convolutional network (MFCN). *Journal of Visual Communication and Image Representation*, 51:201 – 209, 2018.
- [26] K. San Choi, E. Lam, and K. Wong. Source camera identification by JPEG compression statistics for image forensics. In *IEEE Region Conf. TENCON*, pages 1 – 4, 12 2006.
- [27] M. Zampoglou, S. Papadopoulos, and I. Kompatsiaris. Large-scale evaluation of splicing localization algorithms for web images. *Multimedia Tools and Applications*, 09 2016.
- [28] P. Zhou, X. Han, V. I. Morariu, and L. S. Davis. Learning rich features for image manipulation detection. In *The IEEE Conference on Computer Vision and Pattern Recognition (CVPR)*, pages 1053–1061, 06 2018.